INL/EXT-19-55903
Revision 0

Status Report on Separate Effects Testing of Thermal Conductivity of U-Zr Alloy

Cynthia Adkins
Fidelma Di Lemma
Laura Sudderth

September 2019

The INL is a U.S. Department of Energy National Laboratory operated by Battelle Energy Alliance

INL/EXT--19-55903
Revision 0

Status Report on Separate Effects Testing of Thermal Conductivity of U-Zr Alloy

Cynthia Adkins
Fidelma Di Lemma
Laura Sudderth

September 2019

Idaho National Laboratory
Idaho Falls, Idaho 83415

http://www.inl.gov

Prepared for the
U.S. Department of Energy
Office of Nuclear Energy
Under DOE Idaho Operations Office
Contract DE-AC07-05ID14517

ABSTRACT

Phases by definition in an alloy system have distinct physical and chemical properties, including thermal conductivity. The goal of this multi-year study is to show that the different phases present in the U-Zr system indeed do have different thermal conductivities. This study will provide meso-scale (10-100 μm) experimental observations using the Thermal Conductivity Microscope (TCM) of phase dependent thermal conductivity. The results of this study may indicate the need to reconsider the application of homogeneous medium assumption for metallic nuclear fuel that is currently used in fuel performance modeling and could provide input for improving such model using a heterogeneous phase dependent assessment of thermal properties. The local thermal conductivity values from the TCM will be compared to the bulk measurements to validate this work. Twelve alloy samples with varying Zr compositions and heat treatments were fabricated for the initial phase of this study to characterize the individual phases present in the U-Zr system. The gamma body-centered cubic (BCC) phase was successfully identified in the appropriate size for TCM measurement. Next steps in this work will include identification of remaining phases in the U-Zr alloy system. Thermal conductivity will be measured in those phase areas of the materials and used to assess fuel performance codes for improvements.

ACKNOWLEDGEMENTS

The authors would like to thank the Department of Energy's Nuclear Technology Research and Development Program for provided funding and support.

CONTENTS

ABSTRACT iii
ACKNOWLEDGEMENTS v
ACRONYMS ix
1. INTRODUCTION 1
2. Experimental Work 1
2.1 Sample Fabrication 1
2.2 Microstructure Characterization 3
3. DISCUSSION 13
4. FUTURE WORK 13
5. REFERENCES 14

FIGURES

Figure 1. U-Zr Alloy compositions compared to the accepted regions of delta phase. 3
Figure 2. BED images of U-44 wt.% Zr at 200x. Heat treatment identifiers are given on each image. 4
Figure 3. BED images of U-44 wt.% Zr at 500x. Heat treatment identifiers are given on each image. 5
Figure 4. BED images of U-50 wt.% Zr at 200x. Heat treatment identifiers are given on each image. 6
Figure 5. BED images of U-50 wt% Zr at 1000x. Heat treatment identifiers are given on each image. 7
Figure 6. BED images of U-56 wt.% Zr at 200x. Heat treatment identifiers are given on each image. 8
Figure 7. BED images of U-56 wt%. Zr at 500x. Heat treatment identifiers are given on each image. 9
Figure 8. EDS Line scan of 1650-4A-HT3 alloy. 10
Figure 9. BED images of HT3 for all alloys at 200x. 11
Figure 10. EBSD image of Sample 1650-4A-HT3 showing the indexing of the grains and grain boundaries as BCC phase. 12
Figure 11. EBSD image of 1650-4A-HT3 showing similar grain orientation by the inverse pole figure. 13

TABLES

Table 1. Heat Treatment schedule for U-Zr alloys in this study. 2
Table 2. U-Zr alloys Fabricated for this Study, as described in Basak et al. 2

ACRONYMS

AFC	Advanced Fuels Campaign
BCC	Body-Centered Cubic
BED-C	Backscatter Electron Diffraction
EBSD	Electron Backscatter Diffraction
EDS	Energy Dispersive x-ray Spectrometry
FIB	Focused Ion Beam
HCP	Hexagonal Closed Packed
INL	Idaho National Laboratory
LFA	Laser Flash Analyzer (Analysis)
MFC	Materials and Fuels Complex
MOOSE	Multiphysics Object-Oriented Simulation Environment
NTRD	Nuclear Technology Research and Development
SED	Secondary Electron Diffraction
SEM	Scanning Electron Microscopy
TCM	Thermal Conductivity Microscope
TEM	Transmission Electron Microscopy

Status Report on Separate Effects Testing of Thermal Conductivity of U-Zr Alloy

1. INTRODUCTION

Uranium-based metallic fuels are being developed for a variety of nuclear reactors, capitalizing on their high burnup ability, high thermal conductivity, ease of fabrication and ability to be recycled [1,2]. Knowledge of the thermal conductivity of a fuel material is critical for development of new fuel systems and reactor designs. Having data on the thermal conductivity of a fuel both pre- and post-irradiation testing can give insight into the fuel performance in reactor and help with the design of the next set of fuel material tests. Such data will contribute also to the development of a predictive fuel performance model linking microstructure and physical properties for metallic advanced reactor fuels (e.g., MARMOT\MOOSE [3,4,5]). It is, however, extremely difficult to measure the thermal conductivity of an irradiated fuel material due to the high radioactivity of the samples and irregular geometry of the posttest material. Thorough characterization of the physical properties, such as thermal conductivity of the pre-irradiated fuel alloy, will increase the accuracy of the model predicting the thermal conductivity of the post-irradiated fuel; eliminating the need for a perfect geometry, or large samples for bulk measurements that will be extremely hazardous to handle.

In order to assist in the post-irradiated measurement of thermal conductivity, the Advanced Fuels Campaign (AFC) of the Department of Energy's Nuclear Technology Research and Development (NTRD) program has invested in the design and build of a thermal conductivity microscope (TCM) system [6] based upon thermoreflectance methods that is being installed into a remote operation hot cell environment at the Idaho National Laboratory's (INL) Materials and Fuels Complex (MFC). This instrument was specifically designed for the measurement of thermal conductivity on a range of samples having thermal properties that are representative of current fuel systems and advanced accident tolerant nuclear fuels, both fresh and highly radioactive post-test materials. This research project will utilize the capabilities of the TCM along with other characterization instrumentation to investigate the thermal conductivity of the individual phases of the U-Zr alloy system. These measurements can be challenging since the fabrication of single phase U-Zr materials is not trivial and the measurement of the thermal conductivity of the individual phases will be conducted with the TCM.

2. Experimental Work

Phases by definition in an alloy system have distinct physical and chemical properties, including thermal conductivity. The goal of this multi-year study is to show that the different phases present in the U-Zr system indeed do have different thermal conductivities. This study will provide meso-scale (10-100 μm) experimental observations using the TCM of phase dependent thermal conductivity that implicates the need for reconsideration of the application of homogeneous medium assumption for metallic nuclear fuel performance modeling. The local thermal conductivity values from the TCM will be compared to the bulk measurements to validate this work. This work can improve the starting point for the calculation of post-irradiated thermal conductivity of the U-Zr metal fuel system and reduce the frequency of handling highly radioactive metal fuel in quantities large enough for thorough measurements used for industry standard methods such as the Laser Flash Analyzer (LFA).

2.1 Sample Fabrication

Samples of U-Zr alloy were fabricated for this project by arc-casting ingots of U-44 wt.% Zr, U-50 wt.% Zr and U-56 wt.% Zr alloys, sectioning them and annealing them in Zr foil at 1300°C for four hours with a natural cool. This step was conducted to standardize the starting microstructure and is called "as-fabricated" in this report. Samples were then encapsulated in quartz tubes under vacuum, annealed, and water quenched from 875°C, 635°C, and 550°C. Table 1 describes in detail the heat treatment

schedules used for these samples. These temperatures and the associated annealing times come from Basak, et al. [7]. In their paper they discuss similar fabrication methods for generating alloys with our desired U-Zr alloy microstructures (alpha, delta and gamma). Table 2 defines the individual sample IDs and the associated heat treatments. These alloy compositions were chosen due to their vicinity in the phase diagram to the delta-UZr_2 area. The gamma to delta region of the U-Zr phase diagram at approximately 50 wt.% Zr is not well-defined. Due to the difficulty of producing such alloy and limited data available in literature, it is important for this study to test several U-Zr compositions to increase the probability that the delta and gamma single phases will be produced. Figure 1 shows the compositional regions of delta phase on three accepted U-Zr phase diagrams and the alloy compositions that overlap these regions. From this comparison, the alloys in Table 2 were identified for this work. In as many cases as possible, the same sample of alloy will be used for all testing in this plan.

Table 1. Heat Treatment schedule for U-Zr alloys in this study.

Identifier	**Description**
HT1	875°C for 4 hrs, water quench
HT2	875°C for 4 hrs, 720°C for 4 hrs, 635°C for 15 hrs, water quench, 550°C for 10 hrs, water quench
HT3	875°C for 4 hrs, 720°C for 4 hrs, 635°C for 15 hrs, water quench
HT4	As fabricated

Table 2. U-Zr alloys Fabricated for this Study, as described in Basak et al.[7].

Sample ID	**Nominal Composition**	**Heat Treatment**	**Expected Microstructure**
1651-3B-HT1	U-50Zr	HT1	δ + γ phases
1651-3B-HT2	U-50Zr	HT2	δ phase (hcp)
1651-3B-HT3	U-50Zr	HT3	γ phase (bcc)
1651-3B-HT4	U-50Zr	HT4	α + δ + γ phases
1650-1-HT1	U-44Zr	HT1	δ + γ phases
1650-1-HT2	U-44Zr	HT2	δ phase (hcp)
1650-1-HT3	U-44Zr	HT3	γ phase (bcc)
1650-1-HT4	U-44Zr	HT4	α + δ + γ phases
1650-4A-HT1	U-56Zr	HT1	δ + γ phases
1650-4A-HT2	U-56Zr	HT2	δ phase (hcp)
1650-4A-HT3	U-56Zr	HT3	γ phase (bcc)
1650-4A-HT4	U-56Zr	HT4	α + δ + γ phases

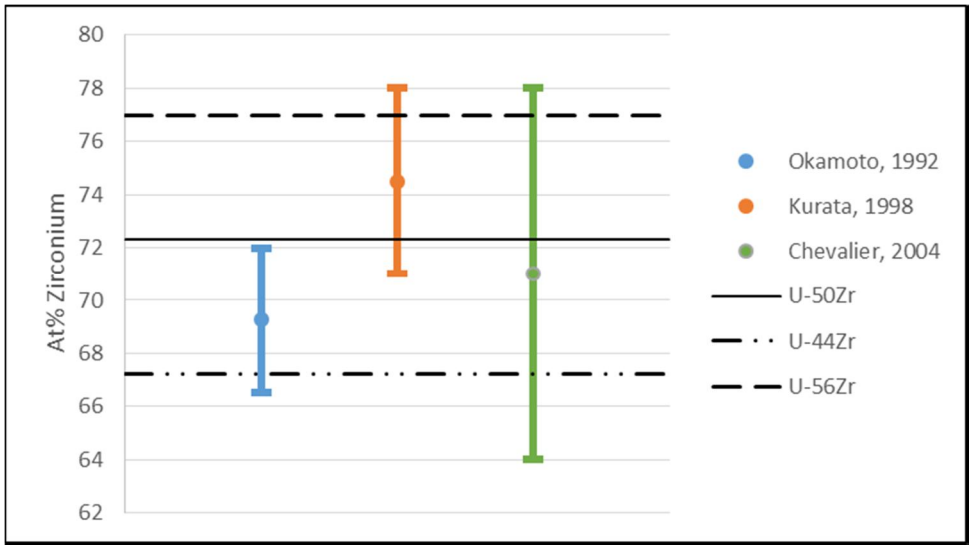

Figure 1. U-Zr Alloy compositions compared to the accepted regions of delta phase [8,9,10].

2.2 Microstructure Characterization

All of the samples listed in Table 2 were sectioned for microstructure characterization. The samples were mounted in epoxy, mechanically polished, and final polished with vibratory method to 0.01 µm. Images were collected using JEOL-IT-500HR Scanning Electron Microscopy (SEM), equipped with an X-Max 50 Energy Dispersive x-ray Spectrometer (EDS), and a Symmetry Electron Backscatter Diffraction (EBSD) camera. Images were taken at 20 kV in both secondary electron diffraction (SED) and backscatter electron diffraction mode (BED-C). Comparisons of the heat treatments for each of the alloy compositions are given in Figure 2–Figure 7. It is observed that as the Zr content increases, the presence of intragranular and grain boundary inclusions also increases in all the heat treatments. The preferential position of the precipitates on the grain boundaries permitted determination of the grain size in most of the samples, which was observed to be over 100 µm. Also note that the large round dark spots on the micrographs in Figure 3 and Figure 4 are actually polishing particles that remained lodged in the surface of the sample and are not large Zr inclusions.

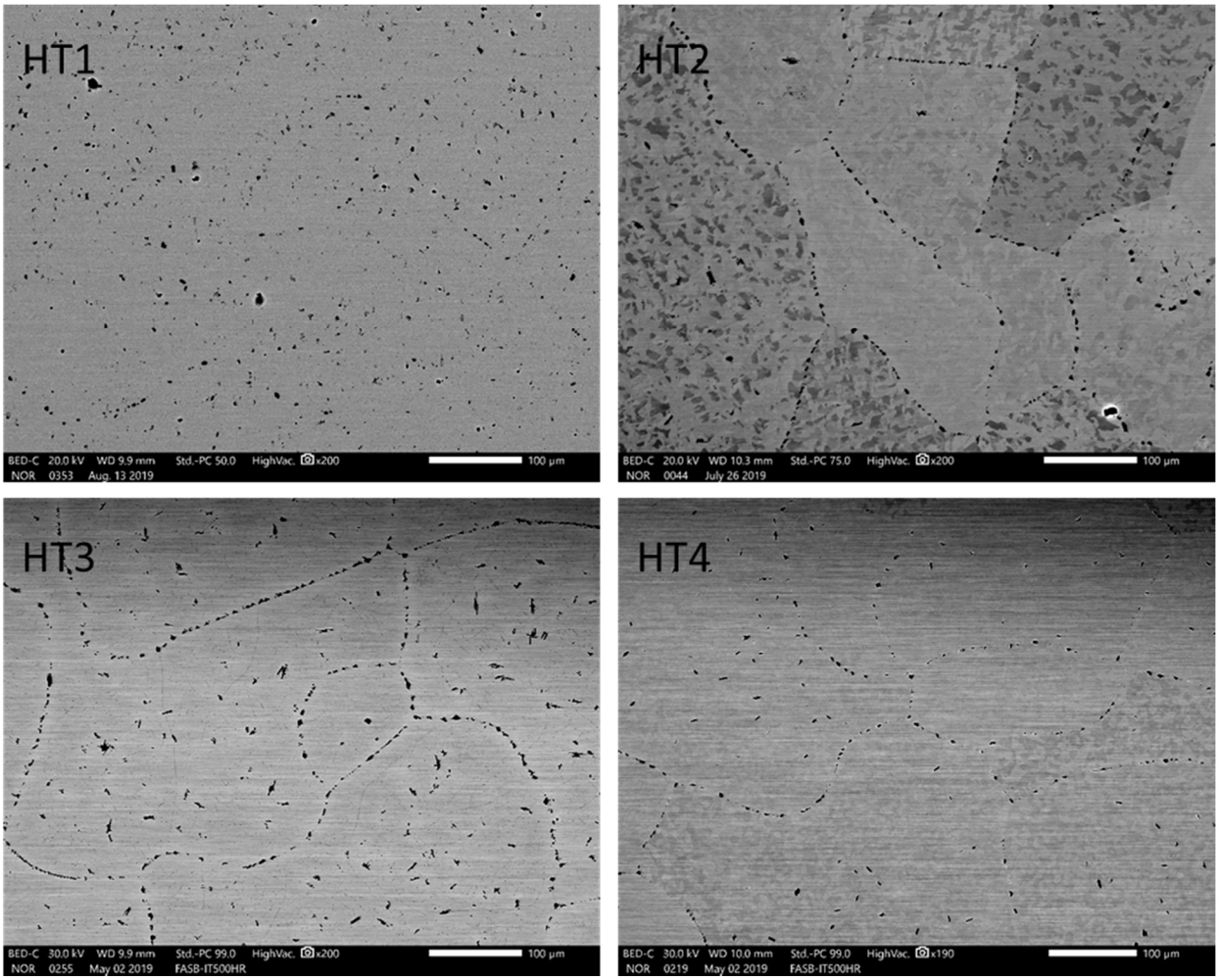

Figure 2. BED images of U-44 wt.% Zr at 200x. Heat treatment identifiers are given on each image.

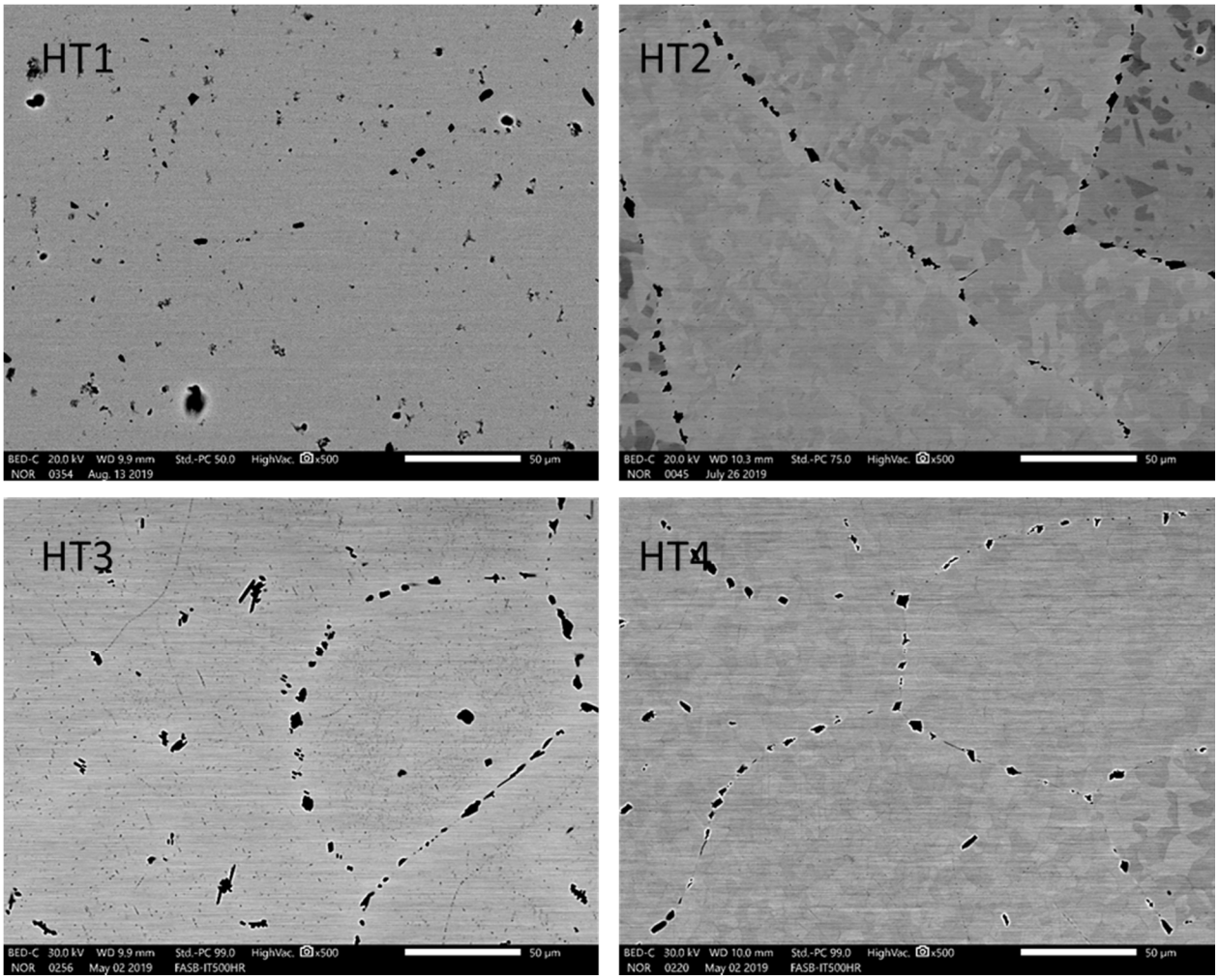

Figure 3. BED images of U-44 wt.% Zr at 500x. Heat treatment identifiers are given on each image.

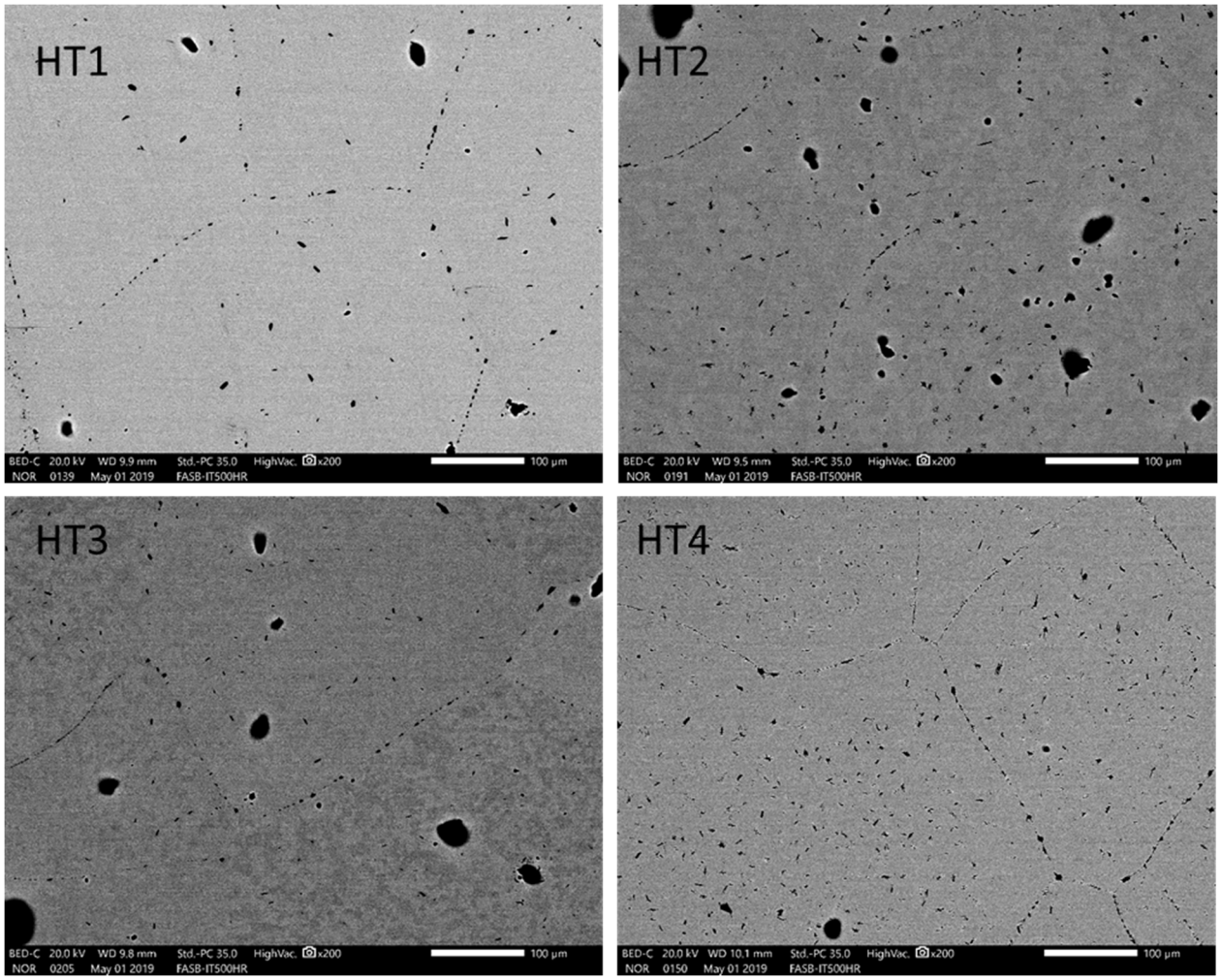

Figure 4. BED images of U-50 wt.% Zr at 200x. Heat treatment identifiers are given on each image.

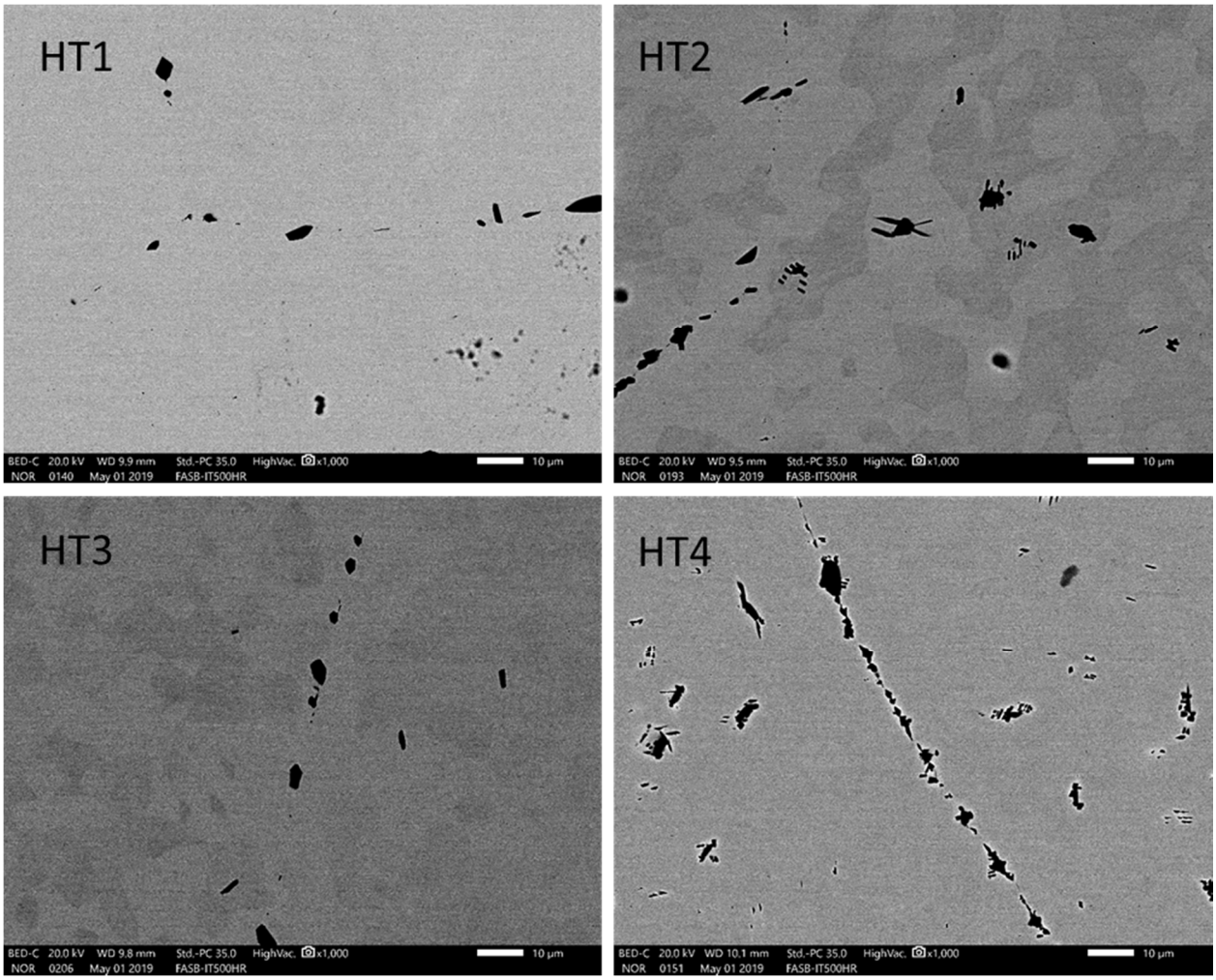

Figure 5. BED images of U-50 wt% Zr at 1000x. Heat treatment identifiers are given on each image.

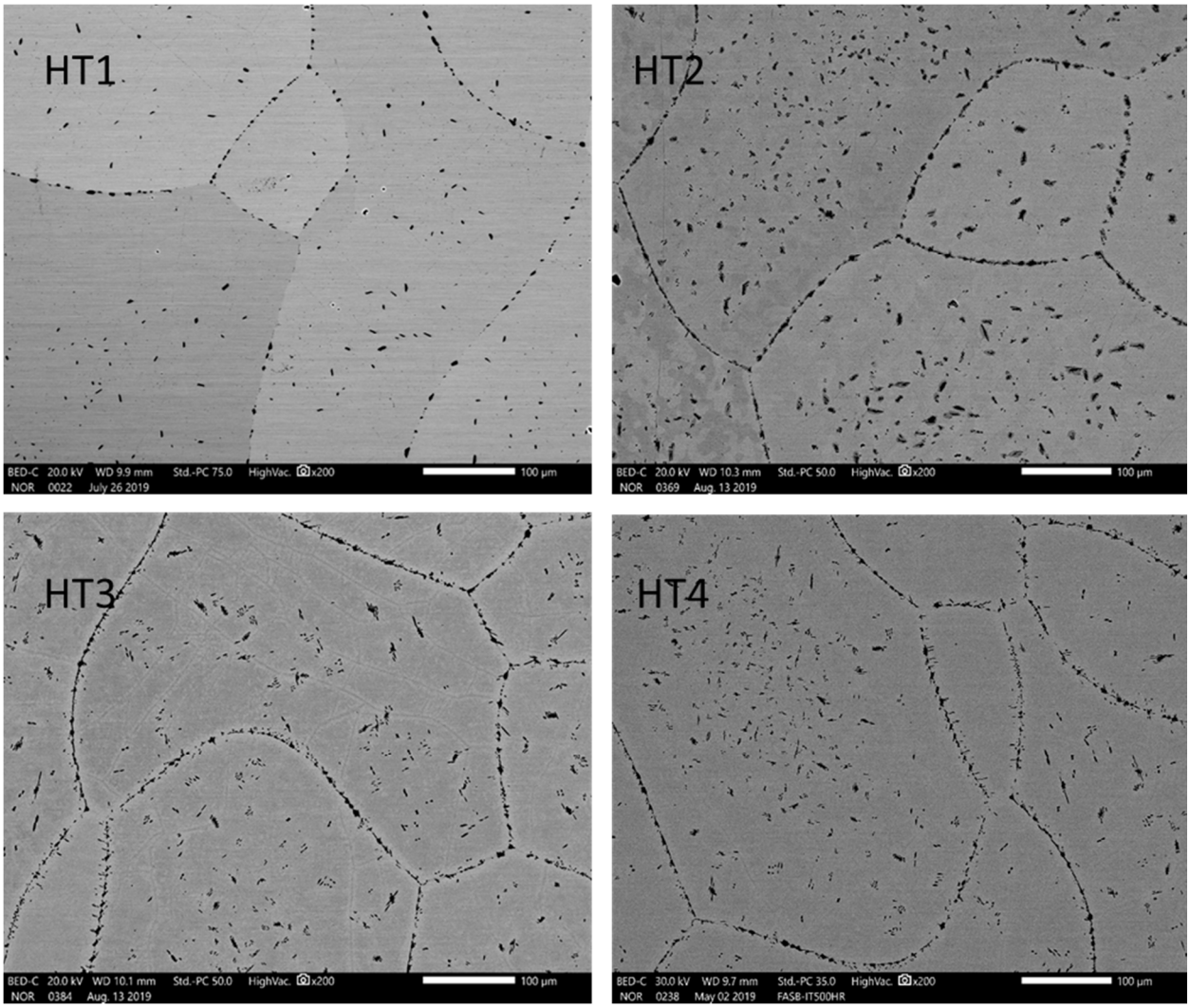

Figure 6. BED images of U-56 wt.% Zr at 200x. Heat treatment identifiers are given on each image.

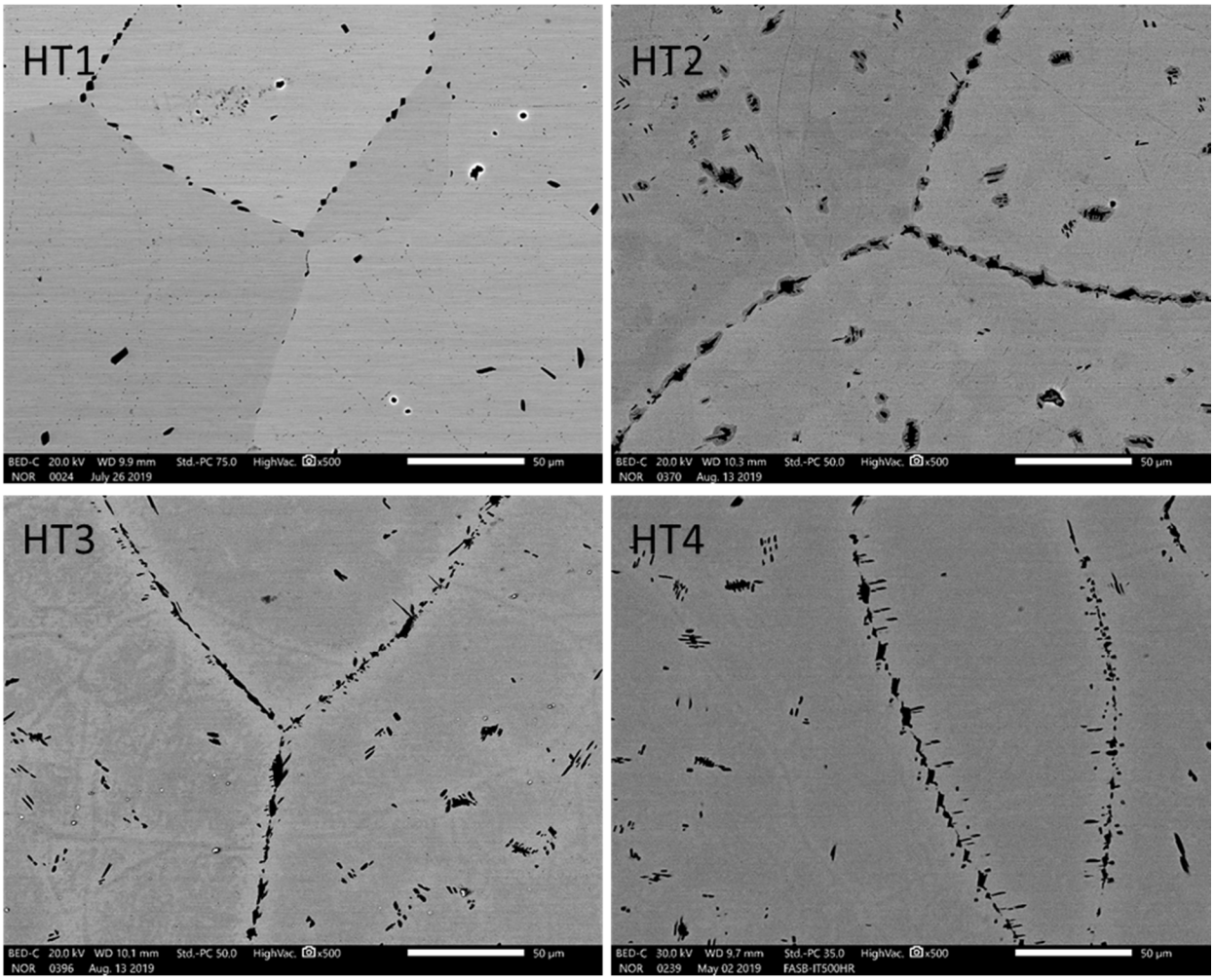

Figure 7. BED images of U-56 wt%. Zr at 500x. Heat treatment identifiers are given on each image.

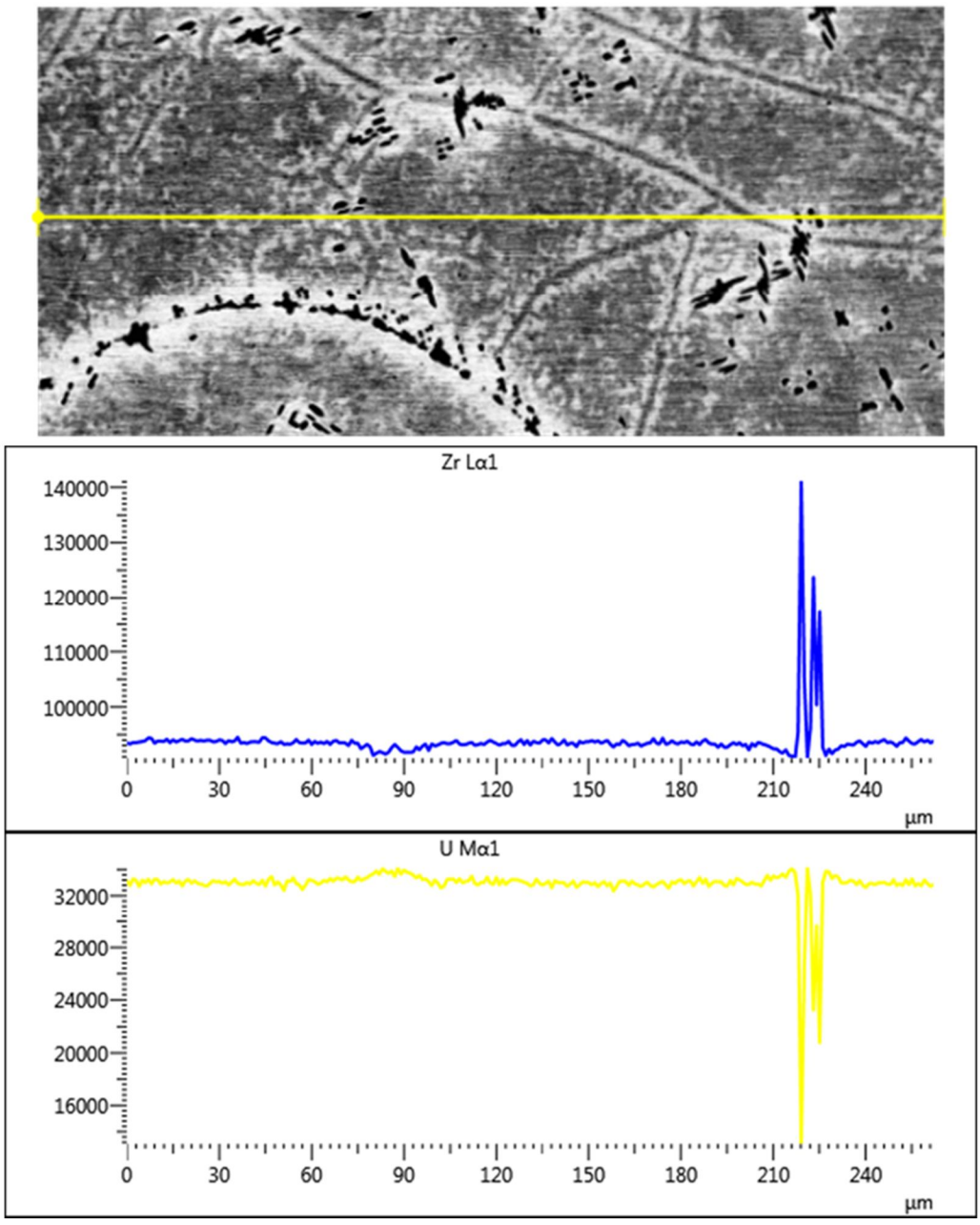

Figure 8. EDS Line scan of 1650-4A-HT3 alloy.

EDS spectra on selected locations for each alloy confirmed that no major compositional changes were present in any of the samples. An example EDS line scan for alloy 1650-4A-HT3 is given in Figure 8. The intensity of the x-rays on the y-axis indicates the level of concentration of U and Zr. Maximizing the contrast shows differences in the grains imaged in the BED-C mode (Figure 2–Figure 7), which is stronger at higher probe current. These differences present as various shades of gray in between different grains. The effect is probably related to electron channeling in the grain. In some samples, within the same grain (e.g. Figure 2. U-44 wt.% Zr-HT2 and HT4) different contrast could be observed (on the scale of <10 µm), implying the presence of sub-grain structure. Heat treatment 3 was designed to quench in the gamma BCC phase of these alloys. Figure 9 shows a comparison of the HT3 samples from each of the alloy samples.

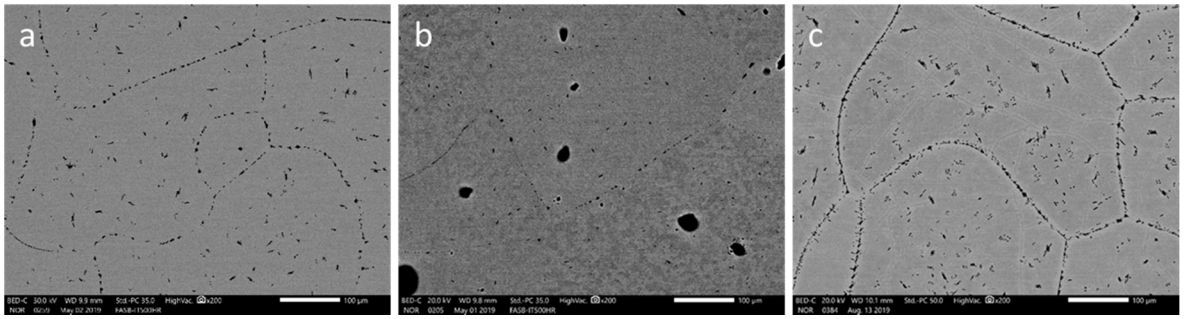

Figure 9. BED images of HT3 for all alloys at 200x.

In order to show the BCC orientation of the gamma phase on samples from HT3, EBSD analyses were conducted. EBSD can determine grain orientation by electron diffraction of the crystalline plane. In particular, this technique was used to determine if the subgrain contrast in the BED-C images came from a difference in composition or orientation. The latter was confirmed on Sample 1650-4A-HT3 (U-56 wt.% Zr), for which EBSD analyses showed disorientation in the major grains (Figure 10), creating a subgrain structure. EBSD on the lower Zr composition was not initially successful. This may be related to poor description of the phases (in particular, lack of good description of the lattice parameters), or to the sample surface. Higher Zr content has been shown to have higher oxidation resistance and, thus, is easier to index [11]. Therefore, only 1650-4A-HT3 is presented. Figure 9c and Figure 10 show the Zr enriched precipitates were observed preferentially on grain boundaries as well. It is worth noting in Figure 11 the close orientation of the grains sampled over an 800 μm^2 areas in the image and the inverse pole figure. This uniform structure may be an indication of a good sample for TCM analysis.

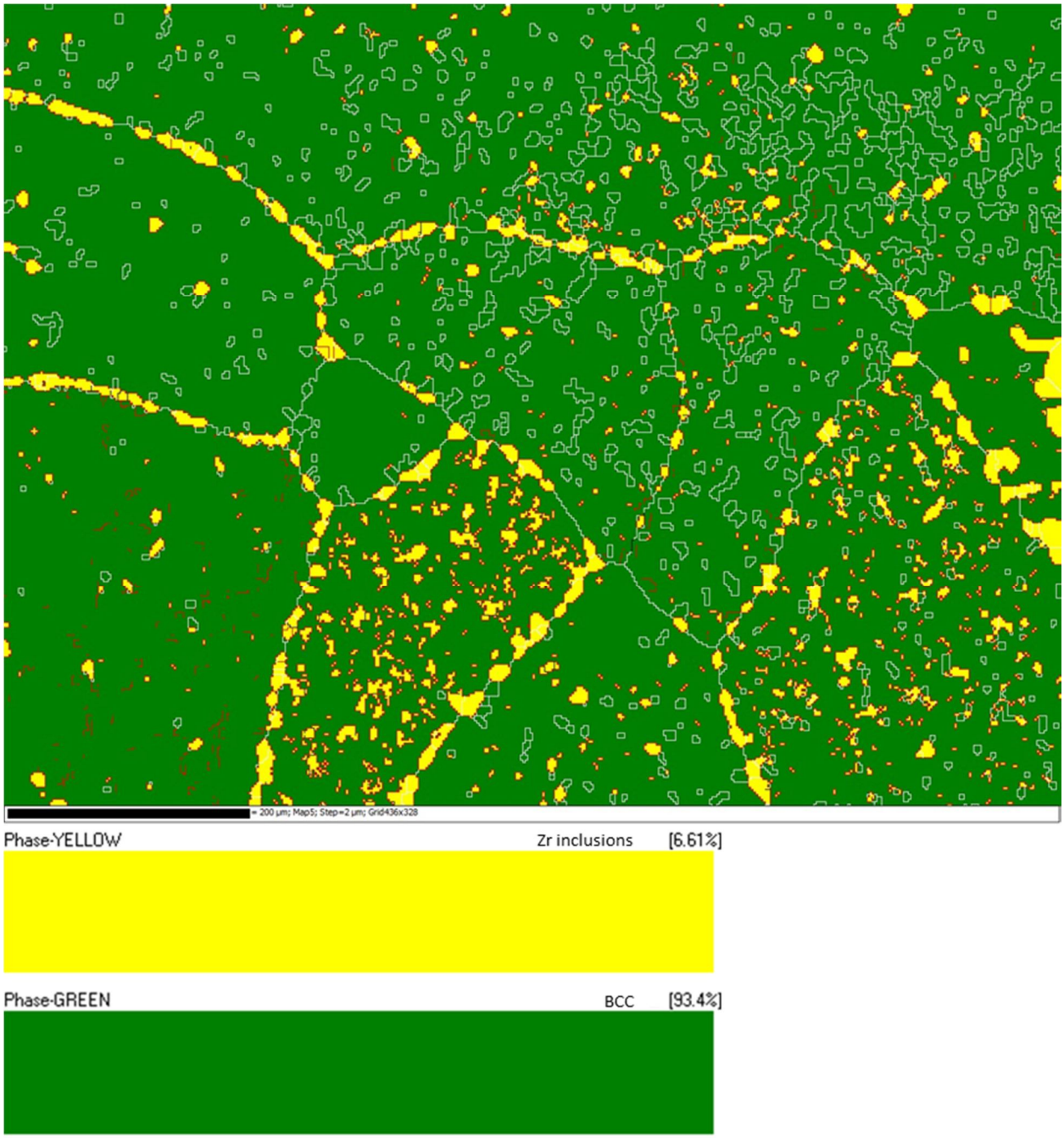

Figure 10. EBSD image of Sample 1650-4A-HT3 showing the indexing of the grains and grain boundaries as BCC phase.

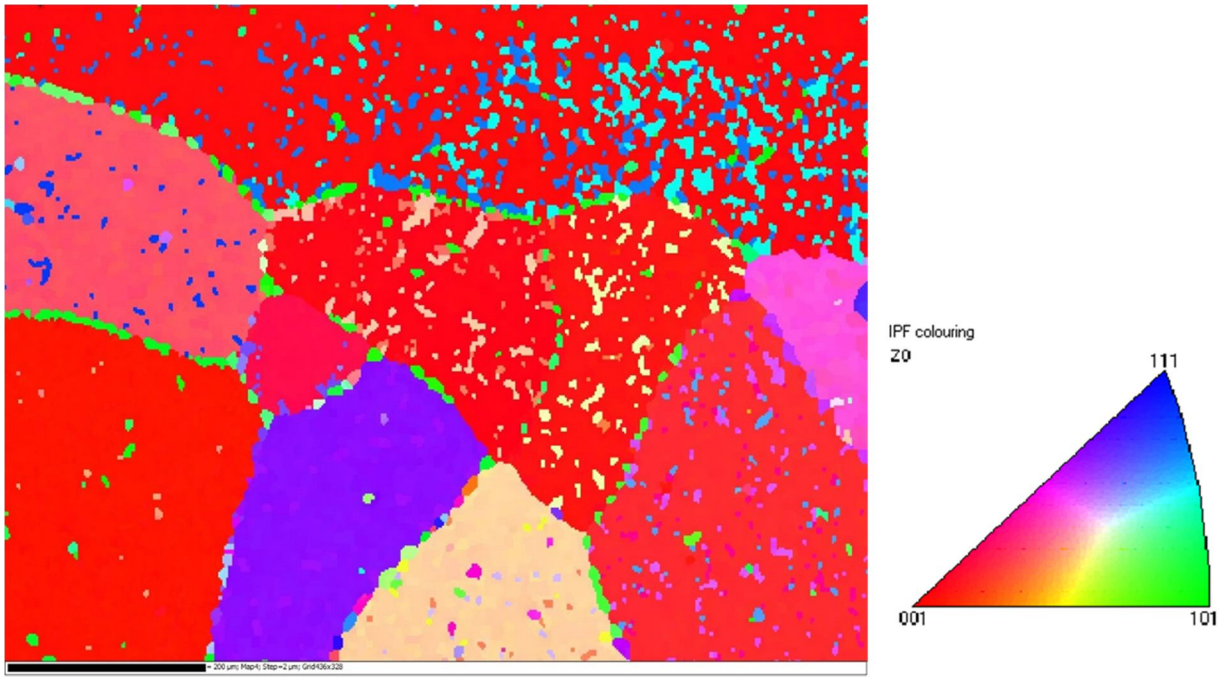

Figure 11. EBSD image of 1650-4A-HT3 showing similar grain orientation by the inverse pole figure.

3. DISCUSSION

The goal of this phase of this study is to fabricate U-Zr alloys with regions of single phase material that are large enough to support a thermal conductivity measurement using the thermoreflectance method on the TCM, approximately 100 µm. While there are many phases in the U-Zr phase diagram, we managed to isolate and identify one of them, the gamma BCC phase with approximately 50-100 µm grain size as indicated by the EBSD data. Other phases of particular interest are the hexagonal closed packed (HCP) delta phase (UZr_2) and the orthogonal alpha-U phase, which present higher challenges. Characterization of additional phases is planned for the next fiscal year using advanced preparation, through use of a focused ion beam (FIB) to eliminate difficulty related to surface effect (e.g. oxidation/distortion) in achieving EBSD analyses. From these studies, we do not expect to see alpha phase in the heat treatments presented here. However, we do expect that HT1 and HT2 will have some delta phase present. Previous works indicate that delta phase is difficult to characterize due to an irregular pattern of U and Zr atoms on the lattice as well as varying composition of the UZr_2 stoichiometry [12,13,14].

4. FUTURE WORK

During this investigation, a course for future work was discovered. Further work in identifying the remaining phases that have been fabricated is needed. A list of items for future investigation is given below. Please note that this is not an all-inclusive list.

1. A more in-depth study of the HT1, HT2 and HT4 samples is needed to reveal the phases present. This will require more measurements of EBSD and TEM to positively identify phases.
2. Investigation into the ability to quantify the amount of phase present by diffraction methods is needed to help with the baseline thermal conductivity model.
3. Development of a fiducial identification system is needed that will allow spatial locations to be reproduced both on the electron microscopes used for phase identification and the TCM. Without

such a technique, the thermal conductivity data cannot be correlated with the appropriate microstructural phase.

5. REFERENCES

1. D. Petti, D. Crawford, N. Chauvin, *Fuels for Advanced Nuclear Energy Systems,* MRS Bulletin, 34(1) (2009) p. 40-45.
2. G. L. Hofman, L.C. Walters, T.H. Bauer. *Metallic Fast Reactor Fuels,* Progress in Nuclear Energy Vol 31 (1-2) (1997) p. 83-110.
3. P. C. Millet, M. R. Tonks, K. Chockalingam, Y. Zhang, S. B. Biner, *Three dimensional calculations of the effective Kapitza resistance of UO2 grain boundaries containing intergranular bubbles,* Journal of Nuclear Materials Vol 439 (2013) pp. 117-122.
4. M. R. Tonks, P. C. Millet, P. Nerikar, S. Du, D. Andersson, C. R. Stanek, D. R. Gaston, D. Andrs, R. Williamson, *Multiscale development of a fission gas thermal conductivity model: Coupling atomic, meso and continuum level simulations,* Journal of Nuclear Materials, Vol 440 (2013) pp. 193-200.
5. M. R. Tonks, D. R. Gaston, P. C. Millet, D. Andrs, P. Talbot, *An object-oriented finite element framework for muliphysics phase field simulations,* Computational Material Science, Vol 51 (2012) pp. 20-29.
6. D. H. Hurley, R. S. Schley, M. Khafizov, B. L. Wendt. *Local measurement of thermal conductivity and diffusivity,* Review of Scientific Instruments Vol 86 (2015)123901.
7. C. B. Basak, N. Brabhu, M. Krishnan, *On the Formation Mechanism of UZr_2 Phase,* Intermetallics, 18 (2010) 1707-1712.
8. H. Okamoto, *U-Zr (Uranium-Zirconium),* Journal of Phase Equilibria, Vol 13 (1992) p. 109-110.
9. M. Kurata, T. Ogata, K. Nakamura, T. Ogawa, *Thermodynamic Assessment of the Fe-U, U-Zr and Fe-U-Zr systems,* Journal of Alloys and Compounds, Vol 271/273 (1998) p. 636-640.
10. P.Y. Chevalier, E. Fischer, B. Cheynet, *Progress in the thermodynamic modeling of the O-U-Zr ternary system,* CALPHAD: Computer Coupling of Phase Diagrams and Thermochemistry, Vol 28 (2004) p. 15-40.
11. Di Lemma et al. ANS Summer 2019.
12. Y. Zhang, X. Wang, G. Zeng, H. Wang, J. Jia, L. Sheng, P. Zhang, *Microstructural investigation of as-cast uranium rich UZr alloys,* Journal of Nuclear Materials vol 471 (2016), pp. 59-64.
13. C.B. Basak, Microstructural evolution of U-rich U–Zr alloys under near-equilibrium condition, Journal of Nuclear Materials, vol 416 (2011), pp. 280-287.
14. S. Irukuvarghula, S. Ahn, S.M. McDeavitt, *Decomposition of the γ phase in as-cast and quenched U-Zr alloys,* Journal of Nuclear Materials, vol 473 (2016), pp. 206-217.